Boundary-Layer Meteorology (2005) 114: 205–231

MEASUREMENT OF AIR TEMPERATURE IN THE PRESENCE OF A LARGE RADIANT FLUX: AN ASSESSMENT OF PASSIVELY VENTILATED THERMOMETER SCREENS

EVYATAR ERELL[1,*], VÍTOR LEAL[2] and EDUARDO MALDONADO[2]
[1]*Jacob Blaustein Institute for Desert Research, Ben-Gurion University of the Negev, 84990 Midreshet Ben-Gurion, Israel;* [2]*Instituto de Engenharia Mecânica, Rua Dr. Roberto Frias, 4200-465 Porto, Portugal*

(Received in final form 26 March 2004)

Abstract. The energy balance of small temperature sensors was modelled to illustrate the effects of sensor characteristics, particularly size, on the accuracy of readings in the presence of strong shortwave or longwave radiant loads. For all but extremely small sensors, radiant exchange may lead to unacceptable errors. The common practice of using passively ventilated instrument screens was evaluated in a series of comparative measurements. The differences resulting from the use of different models of shields may be an order of magnitude greater than the error resulting from sensor calibration. In the absence of technological innovation capable of reducing the error due to radiant exchange to negligible proportions, it is suggested that a standard methodology for calibrating and labelling the error resulting from the characteristics of the screens be adopted, to allow comparison of new data with long-established records.

Keywords: Radiant exchange, Stevenson screen, Temperature measurement.

1. Introduction

The effects of radiant exchange on thermometer readings of air temperature were recognized over 150 years ago, and eventually led to the design of the Stevenson screen in 1864. This white wooden cupboard has since become the standard instrument screen, whereby indirect ventilation is provided through the bottom, double roof and louvered sides, and thermometers placed within it give a close approximation to the true air temperature, undisturbed by the effects of direct solar or terrestrial radiation. However, the Stevenson screen is unsuitable for many applications: it is too bulky and heavy to be portable; it is too large for measurements in confined spaces; it is too obtrusive to be installed in locations accessible to the public; and it may be considered too expensive when a large number of screens is required for simultaneous measurements in different locations.

A variety of radiation screens have been designed in response to these drawbacks. Some are produced commercially, while others have been constructed by researchers to suit budgetary constraints or the specific require-

* E-mail: erell@bgumail.bgu.ac.il

ments of an experiment. Temperature sensors are generally calibrated carefully and their accuracy is specified in most research papers. However, there is no standard procedure for assessing the effect of instrument screens on radiant exchange, and hence on the accuracy of the resulting measurements.

The importance of making accurate readings of air temperature in diverse environments is highlighted in the case of urban climatology, particularly the measurement of urban heat islands. Surface temperatures may be measured remotely using airborne or satellite-based infrared sensors, but mapping air temperatures recorded simultaneously at several locations remains a common technique (Magee et al., 1999; Morris and Simmonds, 2001; Livada et al., 2002). In such studies, the use of identical instrumentation does not guarantee that results are comparable, because measurements are carried out in environments that are inherently different, not least in the exposure to solar radiation. Furthermore, several earlier studies have compared results regarding the urban heat island based on studies in the different cities that used different equipment (Oke, 1973; Grimmond and Oke, 1995).

Accurate measurements of air temperature are also difficult to make where there is a strong temperature gradient in a relatively small distance, especially if the measurement point is exposed to a strong radiant flux or where a radiation screen would interfere with convection. This combination of factors may occur in scale-models of larger elements normally exposed to the environment; in the cavities between glazing elements of modern ventilated facades; and in micrometeorological measurements near the soil or in plant canopies. The use of conventional instrument screens in such cases is not possible, either because they are too large or because their interference with the environment being measured affects conditions too much.

Where electric power is available, mechanically aspirated sensors may overcome some of the difficulties mentioned above, and provide extremely accurate temperature readings. However, while aspirated sensors may be more accurate than non-aspirated ones, they are expensive, their dependence on electric power is a drawback and they, too, interfere with the natural flow of air.

This paper has several aims:

- To illustrate the sensitivity of temperature measurement to radiant exchange, using basic heat transfer calculations and well-established correlations, and to quantify the error as a function of environmental conditions and sensor size.
- To demonstrate experimentally differences in temperature measurements resulting from the use of commercial instrument screens and the Stevenson screen.
- To investigate several cheap, home-made thermometer screens for air temperature sensors, suitable for use in experiments where a large number of sensors is required concurrently.

2. Theoretical Analysis

2.1. Basic heat balance

A temperature sensor may be regarded as a node that exchanges heat with the surroundings by several mechanisms:

- it exchanges heat by convection with the surrounding air;
- it exchanges thermal (longwave) radiation with the surrounding surfaces;
- it may absorb solar radiation (direct and diffuse);
- it may exchange heat by conduction, if it is in contact with a solid, and through the sensor wires.

A basic assumption underlying all temperature measurement is that the size and mass of the sensor, and therefore the Biot Number, are sufficiently small that internal temperature gradients and thermal storage can be neglected. The temperature of a sensor measuring air temperature, i.e. not attached to any surface, may then be calculated from the following heat balance equation:

$$\alpha_{\mathrm{ir}}\sigma(T_{\infty}^4 - T_{\mathrm{s}}^4) + h_c(T_{\mathrm{a}} - T_{\mathrm{s}}) + q''_{\mathrm{solar}}\alpha_{\mathrm{solar}} = 0, \tag{1}$$

where α_{ir} is the absorptivity of the sensor in the infrared part of the spectrum, σ is the Stefan–Boltzmann constant, T_{s} is the temperature of the sensor, T_{∞} is the mean radiant temperature of the surrounding temperature, T_{a} is the temperature of the surrounding air, α_{solar} is the solar absorptivity of the sensor (i.e., to shortwave radiation), and q''_{solar} is the averaged solar radiation flux incident on the surface. In Equation (1), h_{c} is a coefficient of heat transfer between the surface of the sensor and the surrounding air, and is defined in this case as the mean value over the surface of the sensor. Since the sensor is small and the internal temperature gradients are negligible, an average heat transfer coefficient is used, rather than local heat transfer coefficients.

The temperature output from the sensor is T_{s}, while the true temperature (the object of measurement) is T_{a}.

The area-averaged solar flux on the surface of a spherical sensor can be computed from

$$q''_{\mathrm{solar}} = \frac{q_{\mathrm{solar}}}{4\pi R^2} = \frac{1}{2}I_{\mathrm{difh}} + \frac{1}{4}I_{\mathrm{dirn}} + \frac{1}{2}\rho_{\mathrm{g}}(I_{\mathrm{dirh}} + I_{\mathrm{difh}}), \tag{2}$$

where I_{difh}, I_{dirn} and I_{dirh} are the diffuse solar radiation flux on a horizontal plane, the normal beam radiation flux and the direct radiation flux on a horizontal surface respectively, ρ_{g} is the albedo of the ground, and R the radius of the sphere. For a detailed calculation see Appendix A.

Determination of the heat exchange between the surface of the sensor and the surrounding air requires evaluation of the coefficient h_c in Equation (1) above. Boundary-layer theory provides analytical solutions for the value of h_c only for a few well-defined combinations of flow characteristics and object geometries, such as laminar flow over a flat plate. For most other situations, semi-empirical correlations have been developed over the years and used extensively in many engineering applications with excellent results.

These semi-empirical correlations were mostly derived from dimensional analysis combined with experimental wind-tunnel studies. Their applicability to the case at hand rests on the assumption that differences in flow characteristics between the wind tunnel and ambient air in the vicinity of the sensors, especially with respect to turbulence, do not result in unacceptable errors. Two issues need to be addressed in this context:

1. *The characteristics of the atmosphere in the vicinity of the sensor*. Flow in wind tunnels is generally characterized by turbulence that is stationary and homogeneous; flow in the atmospheric boundary layer is usually neither homogeneous nor stationary, except for very short time scales and limited areas. The intensity of turbulence near the surface may range from about 30% in exposed sites (Shiau and Chen, 2002) to 50% or more in the urban canopy layer (Longley et al., 2004). However, turbulence statistics are generally given for time scales of 10–15 min, whereas the relevant time scale in our case is the response time of the sensor – usually on the order of several seconds. Microscale eddies in the atmosphere typically have durations of 10 s to 10 min (Stull, 1988), but the relative spectral intensity decreases substantially at intervals of 30 s or less.
2. *The extent to which turbulence intensity enhances heat exchange from the surface of the sensor*. Several studies of flow over cylinders and spheres show that in fact free-stream turbulence may enhance convective heat transfer between the object and the fluid (Newman et al., 1972; Schlichting, 1979), but give varying estimates of the magnitude of this effect, from 5% to 50% or more. However, the effect is relatively small at low Reynolds numbers (Lowery and Vachon, 1975).

Since the Reynolds numbers under consideration here are very low (typically less than 500), and the time scale in question very short (typically 1–30 s), the error resulting from application of empirical correlations derived from wind-tunnel studies to heat transfer from the surface of sensors exposed to atmospheric turbulence was considered acceptable. Experimental results (see Section 3.1) confirmed the validity of this approach.

The following analysis is based on Whitaker's empirical correlation for heat exchange at the surface of a sphere (Incropera and De Witt, 1990), which was considered the best approximation for the geometry of the sensors

used in the experiment. (Similar empirical correlations may be applied to calculate heat exchange in sensors of other morphologies. The Hilpert correlation, which may be used to assess heat exchange on cylindrical surfaces, is presented in Appendix B.) Thus, the Nusselt number is given by

$$Nu_D = 2 + (0.4Re_D^{1/2} + 0.06Re_D^{2/3})Pr^{0.4}\left(\frac{\mu}{\mu_s}\right)^{1/4}, \tag{3}$$

where Re_D is the Reynolds number, Pr is the Prandtl number, μ the viscosity of air, and μ_s the viscosity of air in the boundary layer near the sensor surface. The Prandtl number for air is about 0.7 for the range of temperatures likely to be encountered in most measurement situations. The viscosity of air is affected by temperature, but assuming that the difference in temperature between the sensor and its surroundings is relatively small (say, less than 10 K), $\left(\frac{\mu}{\mu_s}\right)^{1/4}$ is approximately unity. The expression for forced convection is appropriate since the movement of the air is not provoked by the thermocouple sphere itself, and the Reynolds number falls within the limits of applicability of the correlation, $3.5 < Re_D < 7.6 \times 10^4$ (for air at 300 K and wind speeds less than about 12 m s^{-1}, this assumption is valid if the sensor diameter is less than 10 mm). The Nusselt number is thus (in this case) a function of the Reynolds number only.

The sensor Reynolds number is given by

$$Re_D \approx \frac{UD}{v}, \tag{4}$$

where U is a characteristic velocity, D is the sensor diameter and v the kinematic viscosity of the fluid (in this case, air). While v is related to fluid temperature (the kinematic viscosity of air is approximately 1.4×10^{-5} m^2 s^{-1} at 273 K and 1.6×10^{-5} m^2 s^{-1} at 300 K), for our purposes the Reynolds number depends mainly on the velocity of the flow and on the sphere diameter.

The surface heat exchange coefficient h_c is found from the Nusselt number as follows:

$$h_c = \frac{Nu \cdot k}{D}, \tag{5}$$

where k is the thermal conductivity of the air and D is the diameter of the sensor. Parameterization of h_c in terms of molecular conductivity is justified due to the surface no-slip condition.

2.2. Assessing the error in temperature due to solar radiation

The error due to solar radiation may be assessed in the absence of net longwave radiant exchange. In this case solar energy absorbed exactly equals the heat loss by convection, and Equation (1) becomes simply

$$q''_{\text{solar}}\alpha_{\text{solar}} = h_c(T_s - T_a), \tag{6}$$

and the error is the difference $T_s - T_a = \frac{q''_{\text{solar}}\alpha_{\text{solar}}}{h_c}$. The term h_c is an indication of the rate of heat loss between the sensor and the surrounding air, regardless of the external environmental mechanisms involved in creating air movement. Its value must be determined using an empirical correlation appropriate to sensor shape and flow conditions, as described above.

Figure 1 shows the measurement error due to solar radiation on a hypothetical spherical sensor 1 mm in diameter (such as many thermocouples), assuming a solar absorptivity $\alpha = 0.5$ and no net longwave exchange with the surroundings. (The values for solar radiation are the area-averaged flux over the whole area of the sensor. Thus, a value of $500\,\mathrm{W\,m^{-2}}$ may occur if a sensor is positioned above a highly reflective surface, where it may receive substantial reflected radiation from below in addition to direct solar radiation and diffuse radiation from above.) The need for a radiation screen is evident: at low wind speeds ($U < 3\,\mathrm{m\,s^{-1}}$), the error resulting from solar radiation is between 0.1 and 3 K.

Equations (4) and (5) above indicate that sensor size has a great effect on the surface heat exchange coefficient h_c, and thus on heat loss to the surrounding air. Figure 2 illustrates the effect of sensor size on the error resulting from an area-averaged solar radiation flux of $300\,\mathrm{W\,m^{-2}}$. The sensor is assumed to be spherical and has a solar absorptivity of $\alpha = 0.5$; net longwave exchange with the surroundings is zero. The advantages of small sensor size are obvious: extremely small sensors, such as thermocouples constructed of very fine wire, may have an error of only 0.3–0.5 K even when exposed to relatively intense solar radiation.

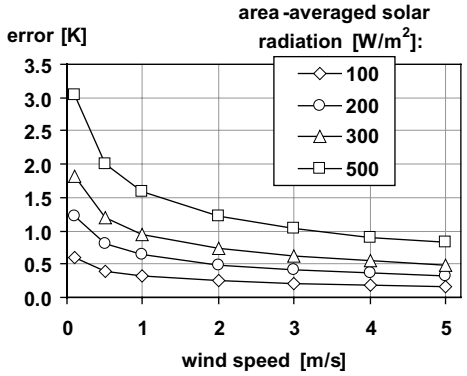

Figure 1. Over-measurement caused by solar radiation as a function of solar flux and air velocity, for a spherical sensor with diameter of 1 mm and a solar absorptivity of 0.5 (in the absence of net longwave radiant exchange).

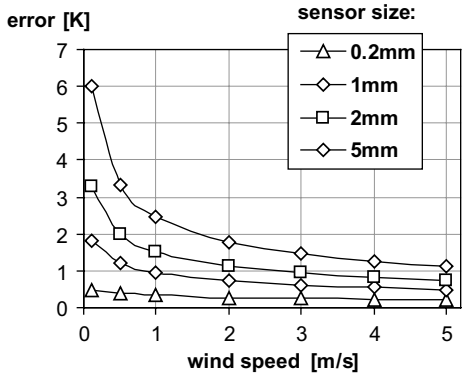

Figure 2. Over-measurement caused by solar radiation as a function of wind speed and sensor size, assuming area-averaged flux of 300 $W\,m^{-2}$ and a solar absorptivity of 0.5 (in the absence of net longwave radiant exchange).

2.3. Assessing the error due to longwave radiation

The error due to longwave radiation can be assessed in the absence of solar radiation, if the temperatures of air and surrounding surfaces are known. In this case we have

$$\alpha_{ir}\sigma(T_s^4 - T_\infty^4) + h_c(T_s - T_a) = 0, \tag{7}$$

where T_s is the sensor temperature (K), T_a is the temperature of air (K), T_∞ the mean radiant temperature of the surroundings (K), σ is the Stefan–Boltzmann constant, approximately $5.67 \times 10^{-8}\,W\,m^{-2}\,K^{-4}$, α_{ir} is the infrared absorptivity of the sensor surface. The difference in temperature between the sensor and the ambient air $(T_s - T_a)$ is in effect the measurement error.

The mean radiant temperature of the surroundings may be calculated from the temperature of terrestrial surfaces and the sky weighted by their respective view factors (see Appendix A, Part 2). To simplify the analysis, an open site will be considered, with an unobstructed view of the sky and of the ground surface. During the daytime, the net area-averaged balance of longwave radiation at the surface of a hypothetical spherical sensor will be relatively small compared to solar radiation. In clear sunny conditions, the ground surface may be substantially warmer than the air, especially if the wind speed is low, but the apparent sky temperature will be much lower than the air temperature. In humid overcast conditions, the ground temperature will be close to air temperature, but the apparent sky temperature will also be only a little below screen temperature.

Unless the sensor is exposed to an unusually hot surface in close proximity to it, the effect of longwave radiation on the measurement of air temperature is thus likely to be largest on clear, dry nights with little or no wind. Under

such conditions, ground surface temperature may be several K lower than screen air temperature, while the sky temperature depression may be as large as 20 K (Martin, 1989). The mean radiant temperature a sensor is exposed to under these conditions may be 10–15 K below air temperature.

Figure 3 illustrates the effect of longwave radiant exchange on temperature measurements made with hypothetical spherical sensors of different sizes in the absence of solar radiation as a function of wind speed, assuming that the sensor reads 288 K, the mean radiant temperature of the environment is 278 K and the sensor surface has an infrared emissivity of 0.5. The magnitude of the error is substantially smaller than that caused by solar radiation. However, since wind speed at night is often quite low, the error may not be neglected unless sensor size is very small.

3. Experimental Analysis

The effect of radiant exchange on temperature sensors was evaluated experimentally in several stages:

(a) The numerical model described above was tested for a sensor with sufficiently large dimensions so that radiant exchange would result in measurable error.

(b) The effect of solar radiation on smaller sensors was evaluated using thermocouples, which are often used in field experiments but not in most standard meteorological stations. They were exposed to direct solar radiation, and were compared to similar sensors in simple cylindrical

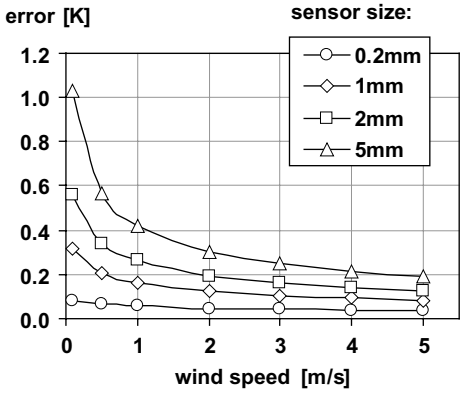

Figure 3. Over-measurement caused by longwave radiation (in the absence of solar radiation), as a function of sensor diameter and wind speed, assuming that the sensor reads 288 K, mean radiant temperature of the environment is 278 K, the sensor surface has an infrared emissivity of 0.5.

radiation shields and to an aspirated sensor serving as a reference. The purpose of this experiment was to confirm the maximum error likely to result from solar radiation when using thermocouples to measure air temperature, and to evaluate the effect of a compact shield intended for monitoring air temperature in a narrow ventilated gap in an experimental glazing system (Erell et al., 2004).

(c) The performance of commercial instrument screens and cheap makeshift screens was then evaluated by comparison of temperature measurements from sensors in these screens, in a standard Stevenson screen and in a mechanically aspirated screen.

Where measurements from a number of sensors were mutually compared, the assumption is that any differences among them were caused by the variable being investigated – in particular, the specific effects of each type of instrument screen being evaluated. The sensors were placed at the same height above a homogeneous surface, a small distance apart, so that individual screens did not obstruct airflow to adjacent ones. While it is possible that atmospheric turbulence could result in instantaneous temperature differences on the order of several tenths of a kelvin in the air surrounding individual sensors, differences in the time-averaged values of high-frequency readings over a period of several minutes are assumed to have been negligible.

The first and third parts of the experiment were carried out on the flat roof of a one-storey building at the Sde Boqer campus of Ben-Gurion University, Israel, in a location unobstructed by trees or other buildings. The experiments with thermocouples were carried out in an open area forming part of the campus of the University of Porto, Portugal.

3.1. Error on an exposed sensor

The temperature sensors used in this part of the experiment were Siemens M841 NTC thermistors. They are almost spherical in shape, with a diameter of 3 mm and thickness of about 1.5 mm, and have a dark maroon colour with an estimated solar absorptivity of 0.8. The sensors have a nominal accuracy of 0.4% and a time constant of approximately 20 s (manufacturer's data). They were calibrated to a tolerance of 0.05 °C at 25 °C. (Because the sensors have a logarithmic response, the calibration was carried out to minimize errors at the anticipated median temperature during the experiment.) Additional environmental parameters measured included wind speed (Met One 010B cup anemometer located about two metres away from the sensor at the same height above the ground), and net radiation (REBS Q*7.1 net radiometer corrected for wind error). Readings were taken at 10-s intervals and 10-min scalar averages were recorded for analysis on a Campbell Scientific

21X data logger. Global horizontal solar radiation (Eppley PSP) and beam normal radiation were monitored at an adjacent meteorological station about 200 m away. The albedo of the ground surface below the sensor was measured and found to be 0.37; its longwave emissivity was assumed to be 0.9.

Figure 4 shows the temperature error of a thermistor exposed to the environment relative to an identical sensor in an aspirated screen over a typical 24-h period. Conditions remained clear and dry throughout the experiment: Maximum global radiation on a horizontal surface was about 1010 W m^{-2}; winds were light – less than 2 m s^{-1} adjacent to the sensors. The measured error was compared with model predictions using Equations (3)–(5) to calculate the coefficient of heat exchange between the sensor surface and the air from wind speed data. The area-averaged net radiant load on the sensor was calculated following the procedure outlined in Appendix A (global horizontal, diffuse and beam solar radiation fluxes were measured directly; environmental longwave radiation was calculated from measurements of net radiation and ground surface temperature; longwave radiation emitted by the sensor itself was calculated from its measured temperature, assuming an infrared emissivity of 0.9). Predicted values match the measured ones closely, with the exception of a period of several hours during the morning, when the measured error was about 1 K lower than predicted.

Model performance statistics (Table I) confirm the impression given by visual inspection of Figure 4. Linear regression with the predicted value as the dependent variable yielded a line of best fit with a slope of 1.02, and an offset of less than 0.2 K. The root-mean-square error (RMSE) of the prediction is not as low as would have been desired (0.49 K), but it is reassuring that most of the error is non-systematic. Finally, the index of agreement

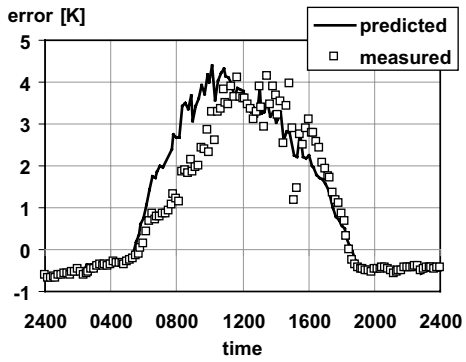

Figure 4. Comparison of predicted temperature error due to radiant exchange with measured differences between a thermistor exposed to the environment and an identical sensor in an aspirated shield.

TABLE I
Model performance statistics.

Statistic	Value
Number of points	289
Observed mean (°C)	0.94
Simulated mean (°C)	1.15
Observed mean − simulated mean (°C)	−0.21
Standard deviation of observed data (°C)	1.52
Standard deviation of simulated data (°C)	1.67
Intercept	0.19
Slope	1.02
Correlation coefficient	0.93
Mean absolute error	0.44
RMSE	0.49
Systematic RMSE	0.21
Unsystematic RMSE	0.62
Willmott index of agreement	0.96

(Willmott, 1981), at 0.96, confirms that the predictions are in fact in good agreement with the observed values.

As expected, the agreement between predicted and observed values is quite good at night, in the absence of solar radiation and with low wind speeds. The relatively poorer agreement during the late morning hours is as yet unexplained, but may be due to an undetected measurement error involving the various radiative fluxes. Another possible source of error in the prediction may be the approximation inherent in the Whitaker correlation, on which the calculation of the convective heat exchange coefficient is based (up to 20%).

3.2. Measurements with exposed thermocouples

Measurements from six thermocouples were made concurrently for a period of about 2 days. Four of the sensors were placed in full sunlight, either exposed or in a radiation shield; two additional sensors were placed beneath the roof of an adjacent open shed about 1 m away but shaded from direct sunlight, as follows:

1. The thermocouple was exposed, i.e., without any protection.
2. The thermocouple was placed inside a mechanically aspirated shield (diameter approximately 12 mm; flow velocity 1.6 m s^{-1}).

3. The thermocouple was placed inside a small cardboard cylinder approximately 14 mm in diameter and 35 mm long covered on the outside with aluminium foil and supported vertically.
4. The thermocouple was placed inside a standard cylinder of the type used (for indoor purposes) in all of the test cells established by the European Union within the PASSYS project to assess the performance of building components (van Dijk, 1993), having a diameter of 68 mm and length of 275 mm.
5. The thermocouple was placed inside a small cardboard cylinder similar to case 3, but in the shadow of the shed roof.
6. An exposed thermocouple was placed in the shadow of the shed roof.

The thermocouples were of the copper-constantan type, with a wire diameter of about 0.5 mm and junction diameter of about 1.2 mm. They were calibrated in a controlled bath to a precision of ± 0.05 °C.

Global and diffuse solar radiation on a horizontal surface were monitored on site with Eppley PSP pyranometers fully calibrated to a primary standard. During the experiment, global radiation reached about 570 W m^{-2} at noon, while diffuse radiation was nearly constant throughout the day at about 70 W m^{-2}. Wind speed during the experiment was in the range 2–7 m s^{-1}, averaging about 3 m s^{-1}.

In the absence of a definitive source of accurate measured temperature representing environmental conditions, temperature measurements from the aspirated sensor are used here as a reference. Results presented are thus of a comparative nature.

Despite the small size of the sensor bead and the low winds, the temperature difference between an exposed thermocouple and a shaded one was substantial in the above conditions, averaging 2.2 °C during a 1-h period between 1300 and 1400 (Figure 5) local time. It appears that the aspirated sensor was affected to a certain extent by solar radiation, too: the thermocouple in the shade of the shed roof averaged 0.8 °C less than the reading from the aspirated one during the period in question.

Protecting the thermocouple from solar radiation by means of a small cylinder (case 3) resulted in only a marginal improvement: during the period in question, the difference between the shielded thermocouple and the one in an identical shield, but located under the shade of the shed roof (case 5), was reduced by 0.2–2 °C during the 1-h period in question (Figure 6).

The effect of radiant exchange is demonstrably weaker at night than during the day, and the average temperature of the shaded thermocouple was almost identical to that measured by the aspirated sensor. However, even in the absence of solar radiation, radiant exchange may not always be negligible: an unshielded sensor exposed to the sky was on the average 0.3 °C colder than a similar one under the shed roof (Figure 7).

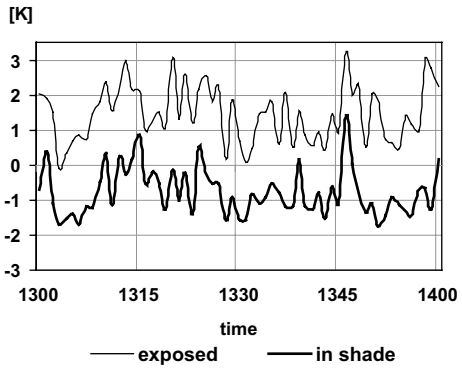

Figure 5. Relative error (K) of temperature readings of two unshielded thermocouples, one of which was beneath a shed roof, compared to readings from a sensor in a mechanically aspirated screen.

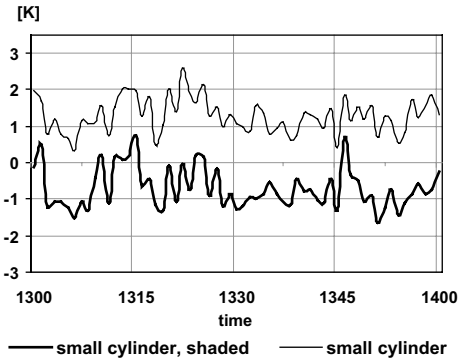

Figure 6. Relative error (K) of temperature readings of two thermocouples shielded in small cylinders, one in the sun and the other shaded, compared to readings from an identical sensor in a mechanically aspirated screen.

3.3. Evaluation of instrument screens

The performance of instrument screens designed to reduce the effects of radiative heat transfer at the sensor surface was next evaluated experimentally by means of concurrent comparative measurements. The monitoring set-up was identical to the one described in Section 3.1 above.

A total of 16 different screens were evaluated in comparison to the Stevenson screen. The screens included two commercial screens manufactured by a leading producer of meteorological equipment, and fourteen makeshift screens. The latter represent different morphologies and were constructed of various materials, ranging from PVC pipes to plastic bowls.

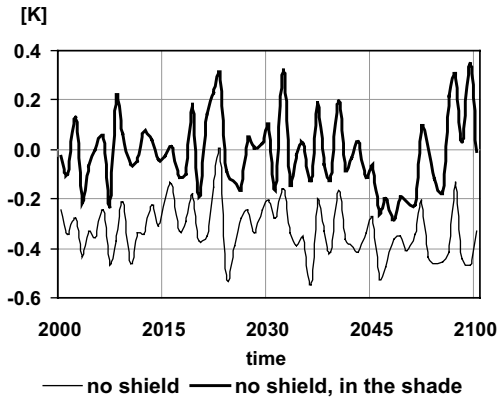

Figure 7. Relative error (K) of temperature readings of two unshielded thermocouples, one exposed to the night sky and the other beneath the shed roof, compared to readings from an identical sensor in a mechanically aspirated screen.

The two commercial screens were of the gill type: the first, a Lambrecht model '814', which will henceforth be referred to as commercial 'Type A', is made of anodized aluminium, 170 mm in diameter and 440 mm high. The second, a Lambrecht model '8141 economy', which will be referred to as 'Type B', is made of white plastic, is 120 mm in diameter and 160 mm high. The selection of commercial screens is by no means exhaustive; it was merely intended to illustrate the differences in temperature measurements that may result from using different screens, even if produced by the same manufacturer.

3.3.1. *Comparison of the Stevenson Screen and Commercial Instrument Screens*

This part of the experiment was carried out over a period of 4 days characterized by stable weather with clear skies and light winds. Results are from typical days, since differences among days were small. Tables with statistical analyses refer to the entire period.

The comparison of temperature measurements taken in the Stevenson screen and in the 'Type A' screen shows substantial differences (Figure 8). In clear sky conditions with global solar radiation in excess of $1000\,W\,m^{-2}$, temperatures in the gill-type screen were 2–2.5 °C higher than in the Stevenson screen. At night, on the other hand, the temperatures in the gill-type screen were up to 1 °C lower than in the Stevenson screen. The differences between the two commercial screens were also substantial: the large, aluminium screen ('Type A') showed consistently higher temperatures during the daytime and lower ones at night (Figure 9).

The discrepancies in temperature between the Stevenson screen and the smaller, lightweight screens may be attributed to differences in radiant ex-

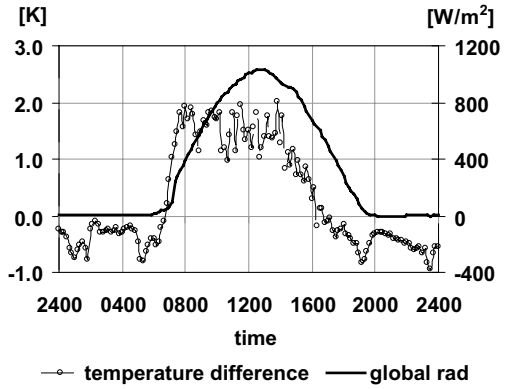

Figure 8. Effect of radiant exchange on temperature readings in the 'Type A' instrument screen relative to the Stevenson screen, on a typical sunny day with light winds. (Negative values indicate the Stevenson screen was warmer.)

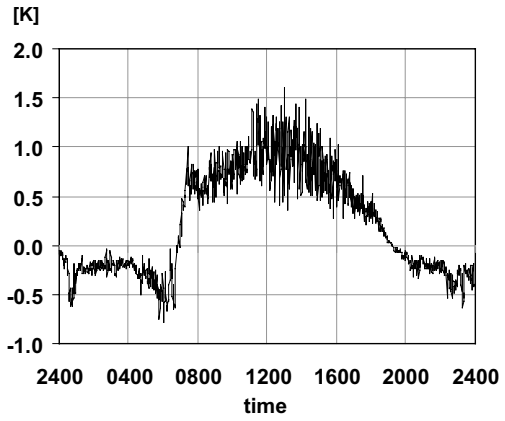

Figure 9. Temperature difference (K) between the two commercial screens on a clear sunny day with light winds. (Negative values indicate temperature in the larger aluminium screen – 'Type A' – were lower.)

change and to the extent to which the sensors are exposed to natural ventilation, but are also concomitant with differences in thermal mass. Such differences would be expected to manifest themselves not only in reduced diurnal amplitude, but also in a time lag and in a reduction in the capacity to respond fully to short-term fluctuations in temperature. The monitoring sequence was thus changed, and while temperature measurements were still taken every 10 s, averages were made every minute. Rather than analyze data over a long period, during which the diurnal pattern would dominate, a 2 h period during daytime, when solar flux was high and wind speed moderate,

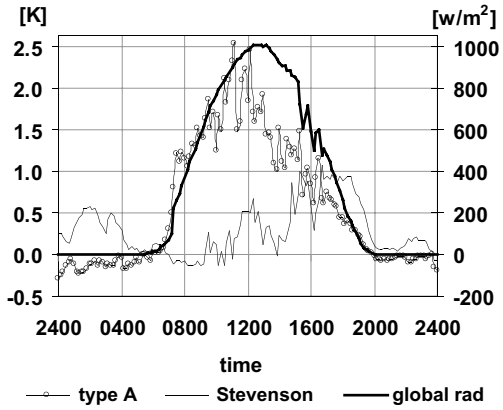

Figure 10. Error in temperature measured in the Stevenson screen and screen 'type A' (relative to a mechanically aspirated screen) on a dry, sunny day with light but constant winds.

was selected for analysis. Between 1300 and 1500, when global solar radiation averaged 935 W m^{-2} and wind speed 2 m s^{-1}, both the standard deviation and the range of temperature in the Stevenson screen were smaller than comparable values for the two commercial screens: 0.39 and 1.72 °C, respectively, compared with 0.51 and 2.42 °C for screen 'type B', and 0.65 and 3.16 °C for screen 'type A'. The time lag is illustrated in Figure 10: following sunrise, temperature in the lightweight commercial screen increases more rapidly than in the Stevenson screen, resulting in a temperature difference of up to 2 °C. For most of the day, temperatures from the Stevenson screen remain about 1.5 °C lower. As solar flux decreases in the afternoon, the lightweight screen cools more rapidly, and the temperature difference is eroded.

Statistical analysis may not always reveal the full extent of differences between the Stevenson screen and modern gill-type screens. Table II shows typical statistical values for temperatures recorded in the Stevenson screen, in the two commercial screens and in a mechanically aspirated double-barrelled

TABLE II
Temperatures measured in different instrument screens (°C).

	Aspirated	Stevenson	Type A	Type B
Mean	22.93	23.23	23.43	23.48
Standard deviation	4.42	4.58	4.81	4.50
Maximum	30.93	31.47	31.84	31.54
Minimum	17.56	17.70	17.49	18.19

shield used as a reference on a sunny day. with light but fairly constant winds of about 1–2 m s^{-1}. As in the previous experiment, there is no 'absolute' reference temperature. However, it was considered that an air speed of about 6 m s^{-1} over both surfaces of the interior shell of the mechanically aspirated shield was sufficient to ensure that the temperature of this shell would be very close to that of the air, resulting in negligible radiant heat transfer from the environment.

Differences between the temperatures recorded in the different screens appear to be quite small – maximum, minimum and mean daily temperatures were about 0.3–0.5 °C higher in the naturally ventilated screens than in the mechanically aspirated one. Yet, as Figure 10 shows, the temperature error in screen 'type A' (defined as the difference relative to the aspirated, double-walled screen) was in fact not negligible for most of the day: it was greater than 1 °C for most of the sunshine hours, and exceeded 2 °C for part of the time.

3.3.2. *Designs for Makeshift Thermometer Screens*

Figure 11 shows schematic drawings of the makeshift screens tested. They may be classified into three general categories, according to the means of providing the sensor with ventilation. Additional variations included the type of exterior finish (glossy white or aluminium foil), and modifications to the basic form to improve protection from direct radiation. Some of the screens, in particular the inverted Styrofoam cup (#9), were included to investigate specific aspects of screen design, even though it was clear *a priori* that that they were not likely to provide adequate protection.

- *Vertical pipes* (cases 1–9 in Figure 11) – these were single-barrelled or double-barrelled, with or without additional shading devices at the top and bottom. This type of screen was expected to allow efficient convective airflow, but less exposure to horizontal flow (wind). The main section of the shield, a vertical pipe, was constructed of either PVC pipe or cardboard, and coated with glossy white paint or aluminium foil. In one variation, the exterior of the pipe was also insulated by means of flexible foam. The pipe was attached to a T-section made of PVC, of a type commonly used in domestic plumbing, with a diameter of 50 or 75 mm.
- *Horizontal pipes* (cases 10–12 in Figure 11) – these were with or without additional shading devices at both ends. This type of screen was expected to allow efficient exposure to wind, provided the pipe was oriented properly, but relatively poorer exposure to vertical flows. The pipes were made of PVC, and coated with glossy white paint or aluminium foil. In one variant, the pipe had lightweight cardboard louvers added to both ends, to reduce penetration of sunlight.

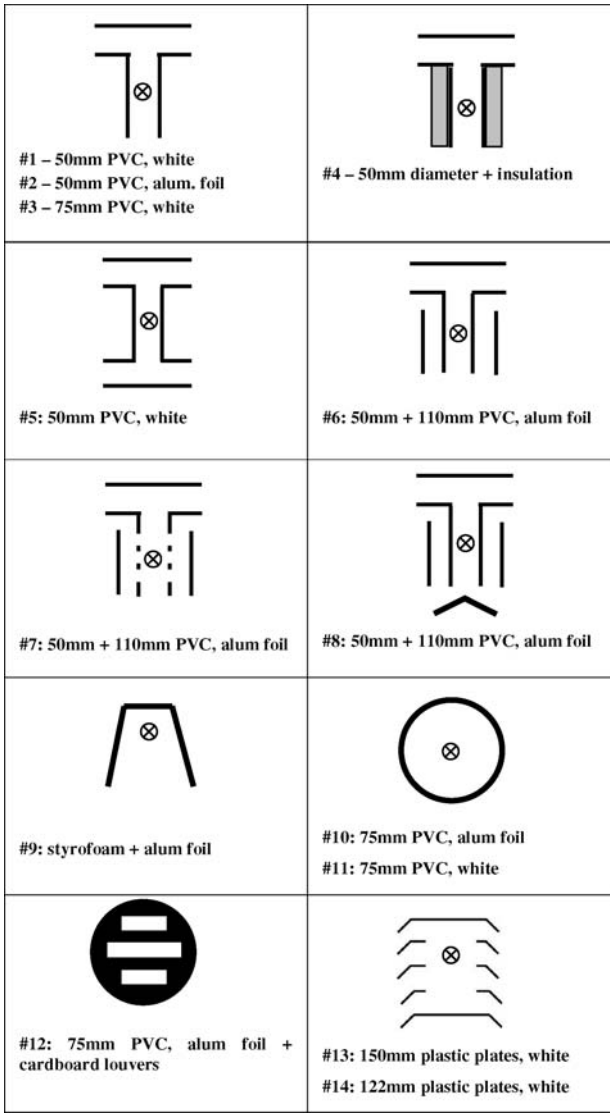

Figure 11. Schematic cross-section through make-shift instrument screens tested.

- *Multi-plate gill-type* (cases 13–14 in Figure 11) – these were of different size. This type of screen, which is also used in most commercial designs, allows multi-directional horizontal airflow, but restricts vertical flow to a certain extent. The screens were constructed of thin plastic soup bowls, with the centre cut out to create a cavity for the sensor (except in the top and bottom bowls). The bowls were painted a glossy white on the exterior surface, and matt black on the interior to minimize the penetration of

reflected light. They were attached by means of threaded metal rods, with thin plastic pipes serving as spacers to maintain a 20-mm gap for ventilation.

Table III summarizes the performance of the various screen designs in comparison with the Stevenson screen in terms of the maximum, minimum and average temperature differences, and the standard deviation of the differences.

The mean temperature recorded in the Stevenson screen over a 4-day period in June, 2002 was lower than that recorded in all of the screens tested, with differences of up to 0.80 °C, except for the inverted Styrofoam cup, whose mean temperature was higher by an average of 2.59 °C. While the discrepancy in the average temperature was relatively small, differences in the maximum temperature were substantial, ranging from 1.8 to 6.8 °C, with the Styrofoam cup again displaying an extreme maximum of 10.6 °C above the Stevenson screen (Figure 12). Minimum temperatures for all of the screens were, however, 1.1–2.1 °C lower than that of the Stevenson screen during the test period (Figure 13).

4. Discussion

The magnitude of errors resulting from radiant exchange at the surface of temperature sensors is too large to be neglected in most environmental conditions. The traditional response to this problem has been to construct instrument screens to block out radiant exchange (as well as provide protection from rain, etc.). Several reports (Sparks, 1972; Andersson and Mathisson, 1992; van der Meulen, 1998) have indicated that this approach, too, is not always capable of producing accurate, reliable and consistent temperature measurements over the whole range of environmental conditions likely to be encountered in field studies. On the other hand, temperature measurements are being made around the world in diverse conditions. In some locations, the guidelines of the World Meteorological Organization for maintaining observing stations cannot be systematically followed for technical or economic reasons.

The problem becomes acute when comparative measurements are carried out at non-standard locations, as is often the case in urban climate studies. The use of identical instrumentation at all sites is insufficient to ensure comparable data, since differences in measured temperature may be the result of varying exposure to radiant exchange that the screens are incapable of preventing. The introduction of corrections to observations requires local measurements of solar radiation and wind speed (at the very least), and risks adding further errors.

TABLE III

Difference in temperature between the instrument screens tested and the Stevenson screen, for a period of four days in June, 2002.

#	Description of shield	Difference in temperature versus Stevenson screen (°C)			
		Mean	Maximum	Minimum	Standard deviation
1	Vertical pipe: 50 mm, T top, white	0.44	2.85	−1.78	1.77
2	Vertical pipe: 50 mm, T top, aluminium foil	0.78	6.76	−1.92	2.15
3	Vertical pipe: 75 mm, T top, white	0.80	5.19	−1.69	1.83
4	Vertical pipe: 50 mm, T top, insulation + aluminium foil	0.44	3.77	−1.79	1.52
5	Vertical pipe: 50 mm, white, T top and bottom	0.52	3.71	−1.15	1.17
6	Double vertical pipe: internal 50 mm, external 75 mm, aluminium foil	0.65	3.76	−1.25	1.32
7	Double vertical pipe: internal perforated 50 mm, external 75 mm, aluminium foil	0.45	2.98	−1.63	1.11
8	Double vertical pipe: internal 50 mm, external 75 mm, aluminium foil, bottom cone	0.37	2.78	−1.51	1.06
9	Inverted Styrofoam cup + aluminium foil	2.59	10.56	−1.25	3.54
10	Horizontal pipe: 75 mm diameter, 500 mm long, white	0.33	4.47	−2.06	1.63
11	Horizontal pipe: 75 mm diameter, 500 mm long, aluminium foil	0.22	2.25	−1.40	0.77
12	Horizontal pipe: 75 mm diameter, 500 mm long, aluminium foil, louvers at ends	0.87	4.78	−1.10	1.61
13	Gill type: 150 mm diameter	0.00	1.76	−1.40	0.65
14	Gill type: 122 mm diameter	0.08	2.04	−1.28	0.79
15	Commercial Type A	0.40	2.81	−1.30	1.08
16	Commercial Type B	0.36	2.38	−1.03	0.87

Negative values indicate that the temperature in the Stevenson screen was higher.

Comparison of temperatures recorded in the Stevenson screen and in lightweight gill-type screens illustrates differences of several types:

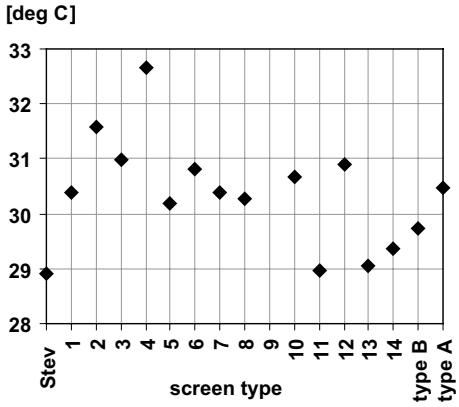

Figure 12. Maximum temperatures recorded in the different instrument screens on a sunny day with light winds (June 6, 2002).

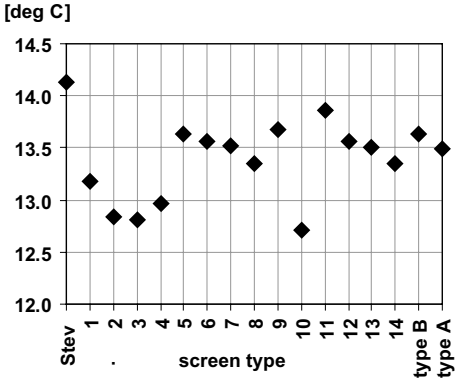

Figure 13. Minimum temperatures recorded in the different instrument screens on a calm, clear night (June 6, 2002).

- differences in daily maxima and minima;
- differences in the sensitivity to short-term temperature fluctuations;
- differences in the response to a changing radiant load.

The characteristics of the shield should therefore be taken into account when analysing the temperature record, especially if detailed data are required at short intervals.

The results of the tests conducted to assess cheap, low-cost thermometer screens indicate that some of the simple designs can provide protection that is the equivalent of that provided by the Stevenson screen or by expensive commercial screens. The following generalizations may be made concerning the designs tested.

- Exposure to horizontal airflow may be more efficient than exposure to vertical flow: of the designs tested, the horizontal pipes and the two variations of the gill-type screens showed lower daytime temperature than the designs based on vertical pipes. Since the screens were all lightweight, the effect of thermal mass is assumed to be negligible; differences in temperature are thus attributed to convective heat loss at the surface of the sensor, which is promoted by higher air speed. Two shield designs that were relatively poorly ventilated – the inverted cup (#9) and the horizontal tube with louvers (#12) – exhibited the highest daytime temperatures.
- The use of shiny aluminium foil at the external surface resulted in lower daytime temperatures than white paint, as illustrated by comparing the two horizontal pipes (#10 and #11), which were otherwise identical. Concurrently, the lower infrared emissivity of the aluminium foil also resulted in higher night-time temperatures in the prevailing atmospheric conditions (clear skies with high net cooling rates), as radiant loss from this shield was less efficient than in the white-painted version.
- While temperature measurements in the two gill-type shields (#13 and #14) were very close to those of the 'Type B' commercial screen, the performance of the aluminium-foil-covered horizontal tube (#11), which is much easier to construct, was nearly as good. In fact, discrepancies between the horizontal tube and the mechanically aspirated screen used as a reference were much smaller than the error recorded in either of the commercial screens (Figure 14). This shield also gave temperatures that were most similar to those made in the Stevenson screen, especially with

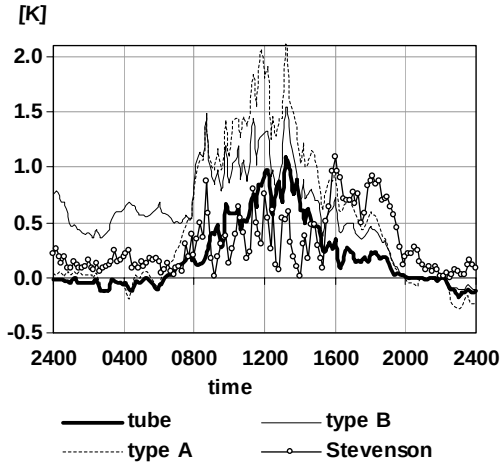

Figure 14. Temperature difference between the horizontal tube with aluminium foil, the two commercial instrument screens and the Stevenson screen, relative to a mechanically aspirated screen, on a typical sunny day (June 6, 2002).

regard to night-time minima. It is worth noting that the exposure of a sensor in the interior of this type of shield to natural ventilation depends to a certain extent on wind direction relative to the longitudinal axis of the pipe. In the experiment reported here, this axis was oriented north-south, to minimize solar penetration in the morning and evening, when solar elevation is low. The prevailing wind was from the north-west, i.e., at an angle of attack of about 45° with respect to this axis, providing sufficient ventilation. However, the directional dependence of both solar protection and ventilation in this type of shield must be considered with respect to anticipated environmental conditions in any experimental program.

Passively ventilated instrument shields are apparently incapable of providing protection from radiant exchange that is sufficient to ensure highly accurate temperature measurements in all conditions. In the absence of calibration procedures for instrument screens – and sufficiently detailed meteorological information on-site to assess the likely measurement error – the best approach to achieving accurate temperature measurement in the presence of high levels of radiation would appear to be the use of very small sensors. As the analysis in the first part of our article shows, the surface convective heat exchange coefficient depends on the size of the sensor. If the sensor diameter is less than about 0.2 mm, the error from full exposure to bright sunshine is estimated to be less than 0.3 K, even at very low ambient wind speed. Such small sensors may be made from very fine thermocouple wire. Although they are relatively fragile, temperature readings made from such sensors are almost free from error due to radiant exchange. They are also suitable for use in restricted spaces, where a radiation shield is too bulky, or where the presence of the shield would alter conditions, especially air flow, to an extent that is unacceptable.

Concurrently, the use of screens whose performance in the presence of strong solar radiation has not been evaluated accurately may lead to unacceptable error. Much of the research in such fields as urban climatology and energy in buildings has been carried out in the past in climates where solar radiation levels are not excessive. However, as more attention is focused on research in tropical or desert climates, the measurement of temperature in the presence of intense solar radiation will require careful planning.

Procedures for homogenizing meteorological records among neighbouring stations, or in a specific station exposed to changing conditions or using different equipment, may account for some of the errors associated with temperature measurement (Peterson et al., 1998). However, data from remote stations are not amenable to techniques based on spatial averaging. Many newly established sites do not provide a sufficiently long historical record. Field studies carried out around the world, in disciplines as diverse as agriculture, urban climatology and solar energy, more often than not have no

historical record to rely upon at all. There is thus a pressing need for a standard procedure that will allow comparison of data assembled using the variety of screens currently in use.

5. Conclusions

Accurate measurement of air temperature in the presence of strong solar radiation presents difficulties that are not easily resolved. The factors affecting errors due to radiant exchange have been analyzed, and the importance of sensor size was shown to be critical in this context. A number of alternative designs for instrument screens were evaluated, yet none was found to give full protection from radiant exchange. However, several cheap homemade screens were shown to as effective as some commercial products. In the absence of perfectly efficient thermometer screens, a universal method of calibrating thermometer screens used in field studies should be adopted, so that errors in measurement resulting from the response of the screen to combinations of environmental factors may be assessed.

Acknowledgements

The authors wish to thank the following persons who provided suggestions for makeshift thermometer screens: Keith Boucher of Loughborough University, U.K.; Scott Chambers of University of Alaska Fairbanks, U.S.A.; Jim Bowers of Langara College, Canada; and Michael Russell, of the University of Tasmania, Australia. Mr. Wolfgang Motzafi-Haller constructed the experimental thermometer screens. Mr. David Klepatch of the Department for Environmental Physics at the Blaustein Institute for Desert Research, Ben-Gurion University of the Negev, provided additional meteorological data.

Appendix A: Modelling the Radiative Exchange at the Surface of a Spherical Sensor Exposed to Solar Radiation

Part 1: Solar radiation

The total solar radiation reaching the sensor surface has three components: direct, diffuse and reflected:

$$q_{\text{solar}} = q_{\text{dir}} + q_{\text{dif}} + q_{\text{refl}}.$$

The exact calculation of the three depends on the geometry of the sensor head and on the directional distribution of the diffuse and reflected radiation. A simple model can be built based on the following assumptions:

- the thermocouple head is a perfect sphere.
- The diffuse radiation is assumed to be isotropic. The flux received by a surface with inclination θ (where $\theta = 0$ implies a horizontal surface facing upwards) is given by

$$I_{\mathrm{dif}} = I_{\mathrm{difh}}\left(\frac{1+\cos\,\theta}{2}\right).$$

- The ground surface is homogenous, with a uniform albedo ρ_{g}. Ground-reflected radiation flux received by a surface with inclination θ is given by

$$I_{\mathrm{refl}} = (I_{\mathrm{dirh}} + I_{\mathrm{difh}})\rho_{\mathrm{g}}\left(\frac{1-cos\,\theta}{2}\right).$$

Each of the flow components can be computed from the measured irradiances: direct horizontal (I_{dirh}), diffuse horizontal (I_{difh}) and direct normal (I_{dirn}), hence

$$q_{\mathrm{dir}} = \int_0^{2\pi}\int_0^{\frac{\pi}{2}}(I_{\mathrm{dirn}}\cos\,\gamma)R^2\sin\,\gamma\,d\gamma\,d\,\varphi = \pi R^2 I_{\mathrm{dirn}},$$

$$q_{\mathrm{diff}} = \int_0^{2\pi}\int_0^{\pi} I_{\mathrm{difh}}\left(\frac{1+\cos\,\theta}{2}\right)R^2\sin\,\theta\,d\theta\,d\varphi = 2\pi R^2 I_{\mathrm{difh}},$$

$$q_{\mathrm{refl}} = \int_0^{2\pi}\int_0^{\pi}(I_{\mathrm{dirh}}+I_{\mathrm{difh}})\rho_{\mathrm{g}}\left(\frac{1-\cos\,\theta}{2}\right)R^2\sin\,\theta\,d\theta\,d\varphi = 2\pi R^2\rho_{\mathrm{g}}(I_{\mathrm{dirh}}+I_{\mathrm{difh}}),$$

where γ is the angle between the normal to the surface at a certain point and the direct incident radiation flux, φ is an azimuth angle, θ is the inclination of the surface at a certain point ($\theta = 0$ is a horizontal surface facing upwards), ρ_{g} is the average albedo of the ground, and R is the sphere radius.

The area-averaged solar flux can be computed from

$$q''_{\mathrm{solar}} = \frac{q_{\mathrm{solar}}}{4\pi R^2} = \frac{1}{2}I_{\mathrm{difh}} + \frac{1}{4}I_{\mathrm{dirn}} + \frac{1}{2}\rho_{\mathrm{g}}(I_{\mathrm{dirh}} + I_{\mathrm{difh}}).$$

Since $I_{\mathrm{dirn}} = \frac{I_{\mathrm{dirh}}}{\sin\,\beta_s}$, β_{s} being the solar height, the expression can be re-written as

$$q''_{\mathrm{solar}} = \left(\frac{1}{4\sin\,\beta_s} + \frac{\rho_{\mathrm{g}}}{2}\right)I_{\mathrm{dirh}} + \frac{1}{2}(1+\rho_{\mathrm{g}})I_{\mathrm{difh}}.$$

Part 2: Longwave radiation

As the sensor is much smaller than its surroundings, the net longwave exchange is given by

$$q_{lw} = A_s \varepsilon \sigma (T_\infty^4 - T^4),$$

where A_s is the surface area of the sensor, ε its emissivity, σ the Stefan–Boltzmann constant, T_∞ the mean radiant temperature of the surroundings and T the temperature of the sensor.

The mean radiant temperature of the surroundings is the temperature of a hypothetical uniform enclosure that would exchange energy with the sensor by radiation at the same rate as the actual environment. It may be estimated as the average of the sky temperature (T_{sky}), ground temperature (T_{grd}) and the temperature of other surrounding surfaces (T_{oth}), weighted by their respective view factors from the sensor and their longwave emissivities, viz.

$$T_e^4 = \frac{f_s \varepsilon_s T_{sky}^4 + f_g \varepsilon_g T_{grd}^4 + f_o \varepsilon_o T_{oth}^4}{f_s \varepsilon_s + f_g \varepsilon_g + f_o \varepsilon_o}.$$

The view factors f_s, f_g and f_o are site specific. In the simplified case of an open rural site, $f_s = 0.5, f_g = 0.5, f_o = 0.0$.

Appendix B: Obtaining the Nusselt Number for a Cylindrical Sensor

If the sensor is encased in a small stainless steel cylinder (of the type often used in thermistors or PT-100 sensors), the Hilpert correlation may be used to obtain the characteristic Nusselt number at the surface:

$$Nu_D = C Re_D^m Pr^{1/3},$$

where the constants C and m are 0.989 and 0.330, respectively for Reynolds numbers in the range 0.4–4; 0.911 and 0.385 for Reynolds numbers between 4 and 40; and 0.683 and 0.466 for Reynolds numbers between 40 and 4,000 (Incropera and De Witt, 1990). The correlation is therefore applicable for wind speeds of up to about $5\,m\,s^{-1}$, even in the case of large sensors with a diameter of 10 mm.

References

Andersson, T. and Mathisson, I.: 1992, 'A Field Test of Thermometer Screens', in *Instruments and Observing Methods Reports No. 49* (*WMO No. 462*), WMO, Geneva, 436 pp.

ASHRAE: 1989, *ASHRAE Handbook – Fundamentals*, American Society of Heating, Refrigerating and Air Conditioning Engineers, Inc., Atlanta, GA.

Erell, E., Etzion, Y., Carlstrom, Sandberg, M., Molina, J., Maestre, I., Maldonado, E., Leal, V., and Gutschker, O.: 2004, 'SOLVENT: Development of a Reversible Solar-Screen Glazing System', *Energ. Build.* **36**, 468–480.

Grimmond, C. S. B. and Oke, T. R.: 1995, 'Comparison of Heat Fluxes from Summertime Observations in the Suburbs of Four North American Cities', *J. Appl. Meteorol.* **34**, 873–889.

Holman, J. P.: 1997, *Heat Transfer*, 8th edn., McGraw-Hill, New York, 688 pp.
Incropera, F. and De Witt, D.: 1990, *Fundamentals of Heat and Mass Transfer*, 3rd edn., John Wiley & Sons, New York, 919 pp.
Livada, I., Santamouris, M., Niachou, K., Papanikolaou, N., and Mihalakakou, G.: 2002, 'Determination of Places in the Great Athens Area Where the Heat Island Effect is Observed', *Theor. Appl. Climatol.* **71**, 219–230.
Longley, I., Gallagher, M., Dorsey, J., Flynn, M., and Barlow, J.: 2004, 'Short-Term Measurements of Airflow and Turbulence in Two Street Canyons in Manchester', *Atmos. Environ.* **38**, 69–79.
Lowery, G. W. and Vachon, R. I.: 1975, 'The Effect of Turbulence on the Heat Transfer from Heated Cylinders', *Int. J. Heat Mass Trans.* **18**, 1229–1242.
Magee, N., Curtis, J., and Wendler, G.: 1999, 'The Urban Heat Island Effect at Fairbanks, Alaska', *Theor. Appl. Climatol.* **64**, 39–47.
Martin, M.: 1989, 'Radiative Cooling', in J. Cook (ed.), *Passive Cooling*, The MIT Press, Cambridge, MA, pp. 138–196.
Morris, C. J. G. and Simmonds, I.: 2001, 'Quantification of the Influences of Wind and Cloud on the Nocturnal Urban Heat Island of a Large City', *J. Appl. Meteorol.* **40**, 169–182.
Newman, L. B., Sparrow, E. M., and Eckert, E. R.: 1972, 'Free-Stream Turbulence Effects on Local Heat Transfer from a Sphere', *Heat Transfer Trans. ASME* **94**, 7–16.
Oke, T. R.: 1973, 'City Size and the Urban Heat Island', *Atmos. Environ.* **7**, 769–779.
Peterson, T., Easterling, D., Karl, T., Groisman, P., Nicholls, N., Plummer, N., Torok, S., Auer, I., Boehm, R., Guillet, D., et al.: 1998, 'Homogeneity Adjustments on *In Situ* Atmospheric Climate Data: A Review', *Int. J. Climatol.* **18**, 1493–1517.
Schlichting, H.: 1979, *Boundary-Layer Theory*, 7th edn., McGraw-Hill, New York, 817 pp.
Shiau, B. and Chen, Y.: 2002, 'Observation on Wind Turbulence Characteristics and Velocity Spectra near the Ground at the Coastal Region', *J. Wind Eng. Ind. Aerodyn.* **90**, 1771–1681.
Sparks, W.: 1972, *The Effect of Thermometer Screen Design on the Observed Temperature*, WMO No. 315, Geneva, 106 pp.
Stull, R.: 1988, *An Introduction to Boundary-Layer Meteorology*, Kluwer Academic Publishers, Dordrecht, 666 pp.
van der Meulen, J.: 1998, 'A Thermometer Screen Intercomparison', in *Instruments and Observing Methods Reports No. 70* (*WMO/TD – No. 877*), *World Meteorological Organisation*, Geneva, 319 pp.
van Dijk, H. A. L.: 1997, 'The PASSYS Test Method to Obtain Thermal and Solar Characteristics of Building Components', in N. Foster and H. Scheer (eds.), *Solar Energy in Architecture and Urban Planning: Proceedings of the Third European Conference on Architecture, Florence, Italy, May 17–21, 1993*, James and James Science Publishers, London, pp. 84–87.
Willmott, C.: 1981, 'On the Validation of Models', *Phys. Geog.* **2**, 184–194.